Supplemental Material for "Contribution of anthropogenic warming to California drought during 2012–2014"

Climate data

The climate data products used in this study are listed in Table S1. Monthly potential evapotranspiration (PET) was calculated using the Penman-Monteith (PM) equation [*Penman*, 1948; *Monteith*, 1965], which is discussed in detail by *van der Shrier et al.* [2011] and Allen et al. [*Allen et al.* [1998]. The climate variables involved in the PM equation are saturation vapor pressure (e_s), actual vapor pressure (e_a), near-surface (2 m) wind speed, and net radiation.

Monthly mean e_s is assumed to be the average of e_s calculated for monthly mean maxiumum daily temperature (T_{max}) and e_s calculated for minimum daily temperature (T_{min}):

$$e_s = a_0+Ta_1 + T^2a_2 + T^3a_3 + T^4a_4 + T^5a_5 + T^6a_6 \quad \text{(eqn. S1)},$$

where T is air temperature in degrees Celsius, e_a is in units of hectopascals (hPa), $a_0 = 6.107799961$, $a_1 = 0.4436518521$, $a_2 = 1.428945805\text{x}10^{-2}$, $a_3 = 2.650648471\text{x}10^{-4}$, $a_4 = 3.031240396\text{x}10^{-6}$, $a_5 = 2.034080948\text{x}10^{-8}$, and $a_6 = 6.136820929\text{x}10^{-11}$ [*Lowe and Ficke*, 1974].

For the PRISM dataset, monthly mean e_a (also in units of hPa) is calculated by applying eqn. S1 to monthly mean dew-point temperature when available. For SHEFF and LDAS, e_a was calculated as:

$$e_a = P(M_{dry}/(M_{h2o} (1/Q-1) + M_{dry})) \quad \text{(eqn. S2)},$$

where Q is specific humidity (kg kg^{-1}), P is surface pressure (hPa), M_{h2o} is the atomic weight of water (18.01534) and Mdry is the atomic weight of dry air (28.9644).

Grids of monthly precipitation total, T_{max}, T_{min}, e_s, e_a, wind speed, and insolation were bilinearly interpolated to have the geographic resolution of PRISM (~4 km). For each variable, datasets were then calibrated to a common set of monthly climate normals during 1961–2010. For precipitation, all grids were converted to fractions of the climatological monthly mean, interpolated to PRISM resolution, and then multiplied by the climatological monthly mean of the target dataset (target datasets provided below). For the other variables, grids were converted to monthly z-scores (each month had a mean of zero and standard deviation of one during 1961–2010), interpolated to PRISM resolution, and multiplied by the climatological monthly means and variances of the target dataset.

It was necessary to interpolate all datasets to a common spatial resolution because the datasets were combined with one another in all possible combinations for the calculations of PET and the self-calibrated Palmer Drought Severity Index ($PDSI_{sc}$). It was necessary to calibrate the means and variances of the downscaled time series to accurately represent the effect of topography on precipitation and PET. While the TopoWx, PRISM, and VOSE datasets all have very fine native spatial resolutions (~800 m to ~5 km), other datasets such as GPCC or NOAA PREC/L have low native spatial resolutions of 0.5° to 1.0°, leading to vastly different means and variances in areas of complex topography. This, if uncorrected, would be problematic in

calculations of water balance. For example, a precipitation record representing a 1.0° grid cell in a topographically complex area would over-represent mean and variability at low elevations within the grid cell, artificially enhancing the probability of soil saturation and runoff in those places. The opposite problem would be the case for high elevations within the grid cell. Target datasets for calibration were PRISM for precipitation, TopoWx for temperature, PRISM for vapor pressure, and LDAS for wind velocity and insolation (LDAS datasets described below). TopoWx is used as the target dataset for temperature because this dataset was recently reported to make advancements in the accuracy of temperature means, variances, and trends at high elevation in the western United States [*Oyler et al.*, 2015]. Monthly grids of PRISM dew point are not yet available for the most recent version (LT81m) of the PRISM dataset (http://prism.nacse.org) and instead come from an older version (LT71m) that is still updated monthly (http://oldprism.nacse.org). The new version of PRISM does provide monthly climatological mean fields for dew point from 1981–2010 (version Norm81m), allowing us to additively adjust the monthly PRISM dew point grids to match these mean fields during 1981–2010.

The most recent GPCC v7 precipitation dataset covers 1901–2013 and is extended through 2014 using the GPCC v4 monitoring product. The v7 dataset is available with spatial resolutions of 0.5° and 1.0° but the v4 dataset is only available with 1.0° resolution. We appended the v4 data for 2014 to the v7 1.0° dataset and downscaled to PRISM resolution. We found that this downscaled dataset agreed well with the downscaled 0.5° version during the overlapping period of 1901–2013 in terms of statewide mean water-year precipitation totals. We extended the downscaled dataset that was based on the 0.5° data by appending the downscaled 2014 data based on v4.

The LDAS and NCEP data products were compiled from multiple datasets in order to extend temporal representation. LDAS comprises data from: 1) version 2 of the National Land Data Assimilation (NLDAS-2) for 1979–2014; and 2) version 2 of the Global Land Data Assimilation (GLDAS-2) for 1948–1978. For all three LDAS climate variables used (vapor pressure, wind speed, and insolation), both NLDAS-2 and GLDAS-2 were first bilinearly interpoltated to the geographic resolution of PRISM. GLDAS-2 annual time series for each grid cell and month were then calibrated to match the means and variances of NLDAS-2 during the common period of 1979–2010. The NCEP dataset was compiled similarly and comprises data from: 1) the National Center for Environmental Protection-Department of Energy Reanalysis 2 (NCEP-DOE2) for 1979–2014; 2) the NCEP/National Center for Atmospheric Research (NCEP/NCAR) Reanalysis for 1948–1978; and 3) the National Oceanic and Atmospheric Administration (NOAA) 20th Century Reanalysis for 1895–1947. For both NCEP climate variables used (wind speed and insolation), NCEP/NCAR were calibrated to NCEP-DOE2 during their overlap period from 1979–2014, and then the resultant dataset for 1948–2014 was used to calibrate the NOAA 20th Century Reanalysis data during the overlap period from 1948–2012. The final NCEP wind speed and insolation datasets were then calibrated to match the means and variances of LDAS during 1961–2010 for each grid cell and month.

As described in the article, the data products considered are in some cases not produced independently, particularly for humidity, wind speed, and insolation. For example, the GLDAS2 data come from the *Sheffield et al.* [2006] dataset (SHEFF), and the SHEFF dataset is based

largely on the NCEP/NCAR dataset during 1948–2012 [*Kalnay et al.*, 1996] before adjustments to remove some biases and improve agreement with observations. The NLDAS2 data come from the NCEP North American Regional Reanalysis (NARR) [*Mesinger et al.*, 2006], which is a modeled product that uses the NCEP-DOE2 Reanalysis for boundary conditions. For the SHEFF and NLDAS2 insolation, both datasets are bias corrected to match the monthly climatological means of the satellite-based NASA/GEWEX Surface Radiation Budget dataset [*Gupta et al.*, 2006]. (See the Supplemental section of Sheffield et al. [2012] for a more detailed description of the compilation of the SHEFF solar dataset.) Thus, there is circularity among the humidity, wind speed, and insolation data products used in this study that limits the degree to which the spread among data products actually characterizes ranges of uncertainty. For all humidity, wind speed, and insolation datasets, the methods of production varied over time and the reader is referred to the documentation referenced in Table S1 for details.

As stated above, monthly net radiation (R_n) is one of the variables used to calculate monthly PET. R_n is calculated as net downward shortwave radiation (SW_d) minus net upward longwave radiation (LW_u). SW_d is calculated as insolation (from the datasets listed in Table S1) multiplied by one minus the surface albedo. We assume that surface albedo follows the mean annual cycle established for each grid cell according to the Noah land surface model when forced by NLDAS-2 meteorology [*Xia et al.*, 2012]. In reality albedo varies interannually, largely as a result of variations in snow cover and vegetation, but estimations of albedo variations prior to 1979 are likely to be highly uncertain. A sensitivity test nevertheless showed that post-1979 variations in albedo have a near zero effect on $PDSI_{sc}$ records.

We estimate LW_u following *Allen et al.* [1998]. Briefly, LW_u is a function Stefan-Boltzmann black-body radiation (exponential function of near-surface temperature) multiplied by an estimate of atmospheric emissivity. This quantity is estimated as a function of atmospheric vapor pressure and cloudiness, where cloudiness is estimated from the fraction of available shortwave radiation that makes it to the surface.

It was important that all calculations of $PDSI_{sc}$ were carried out over the same time period (1901–2014) because the $PDSI_{sc}$ value for a given month is affected by past and future climate and because $PDSI_{sc}$ was calculated based on the calibration period 1931–1990, which extends prior to the beginning of some climate datasets. We therefore artificially extended datasets that did not cover the entire 1901–2014 period using alternate datasets. No calibration was necessary for this step because all datasets already had matching means and variances during 1961–2010. PREC/L precipitation and TopoWx temperature were extended with VOSE. SHEFF vapor pressure was extended with PRISM. For wind velocity and insolation, SHEFF was extended for 2013–2014 with LDAS, and LDAS was extended for 1901–1947 with SHEFF. All records of $PDSI_{sc}$ and PET presented in the article exclude values produced with artificially extended climate datasets.

Table S1: Climate datasets

Variable	Abbrev.	Full Name	Years	Reference(s)
Precipitation				
	VOSE	NOAA Vose et al.	1895–2014	*Vose et al.*, 2014
	PRISM	Parameter-elevation Regressions on Independent Slopes Model	1895–2014	*Daly et al.*, 2004
	GPCC	Global Precipitation Climatology Centre: version 7 (for 1895–2013), version 4 monitoring product for 2014	1895–2014	*Schneider et al.*, 2014
	PREC/L	NOAA's Precipitation Reconstruction over Land	1948–2014	*Chen et al.*, 2002
Temperature				
	VOSE	NOAA Vose et al.	1895–2014	*Vose et al.*, 2014
	PRISM	Parameter-elevation Regressions on Independent Slopes Model	1895–2014	*Daly et al.*, 2004
	BEST	Berkeley Earth Surface Temperature	1895–2014	*Rohde et al.*, 2013
	TopoWx	Topography Weather	1948–2014	*Oyler et al.*, 2015
Vapor Pressure				
	PRISM	Parameter-elevation Regressions on Independent Slopes Model	1895–2014	*Daly et al.*, 2004
	SHEFF	Princeton Global Meteorological Forcing Dataset version 2	1901–2012	*Sheffield et al.*, 2006; *Sheffield et al.*, 2012
	LDAS	Land Data Assimilation System: Combination of - [1]NLDAS-2 for 1979–2014 - [2]GLDAS-2 for 1948–1978	1948–2014	[1]*Mitchell et al.*, 2004, [2]*Rodell et al.*, 2004
Wind velocity and Insolation				
	LDAS	Land Data Assimilation System: Combination of: - [1]NLDAS-2 for 1979–2014 - [2]GLDAS-2 for 1948–1978	1948–2014	[1]*Mitchell et al.*, 2004, [2]*Rodell et al.*, 2004
	SHEFF	Princeton Global Meteorological Forcing Dataset version 2	1901–2012	*Sheffield et al.*, 2006; *Sheffield et al.*, 2012
	NCEP	Combination of products: - [1]NCEP-DOE 2 for 1979–2014 - [2]NCEP/NCAR Reanalysis for 1948–1978 - [3]NOAA 20th Century Reanalysis for 1895–1947	1895–2014	[1]*Kanamitsu et al.*, 2002, [2]*Kalnay et al.*, 1996, [3]*Compo et al.*, 2011

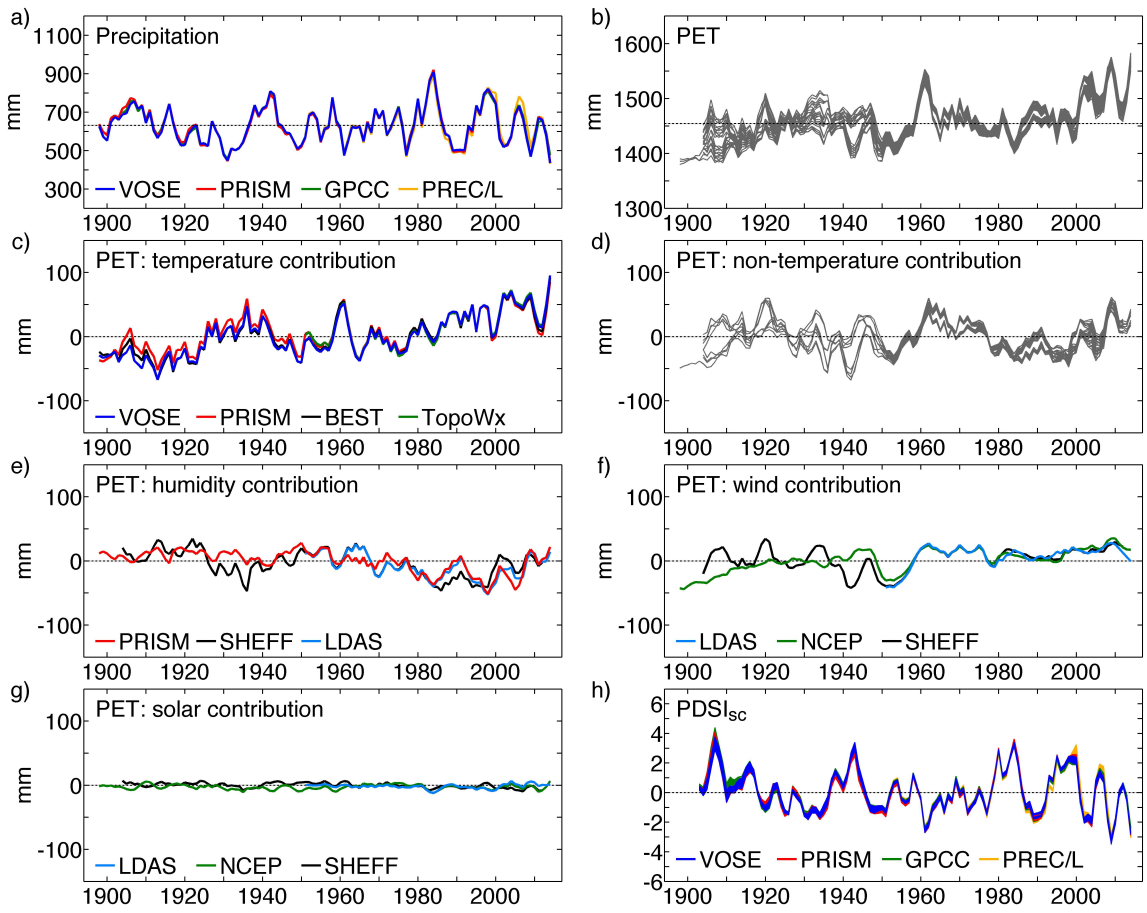

Figure S1. As in Figure 1, but for 3-year running averages. (a) Water year (WY) precipitation. (b) WY potential evapotranspiration (PET) totals, calculated using the Penman-Monteith equation for all combinations of 4 temperature, 3 humidity, 3 wind velocity, and 3 insolation datasets. (c) Temperature contribution to WY PET anomalies. (d–g) Contributions of (d) all non-temperature variables, (e) humidity, (f) wind velocity, and (g) insolation to WY PET anomalies. (h) Summer (June–August) $PDSI_{sc}$ calculated with all combinations of the climate-variable datasets. Colors are as in (a). Horizontal black lines: 1931–1990 means. Colors distinguish data products.

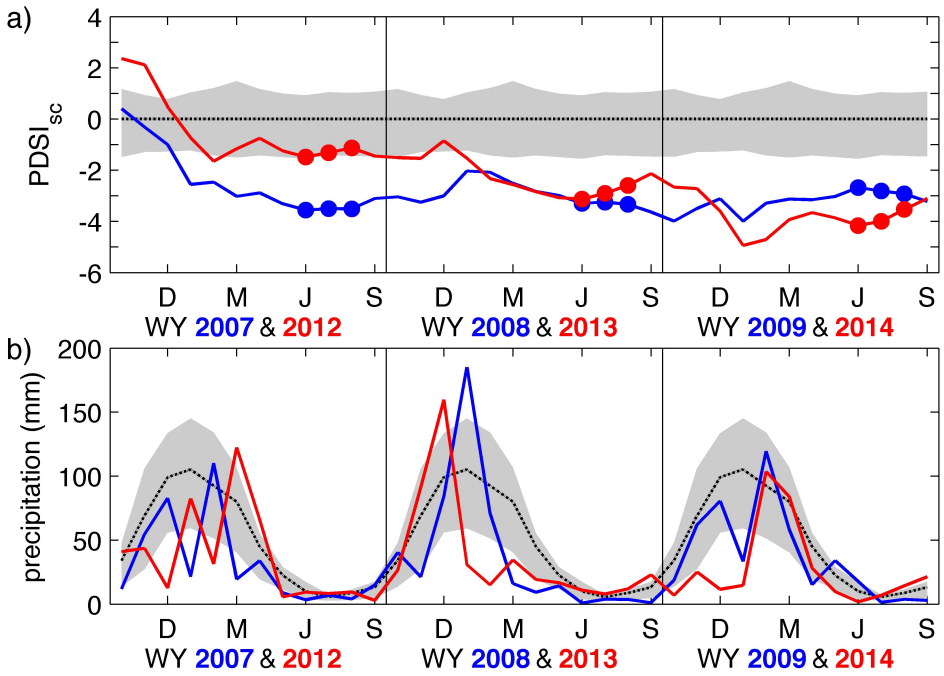

Figure S2. Monthly $PDSI_{sc}$ and precipitation during three-year droughts: (blue) WY 2007–2009 and (red) WY 2012–2014. Black dotted line and shading: 1931–1990 mean and interquartile conditions. Dots indicate June, July, and August, the months used to calculate summer $PDSI_{sc}$ in this study. Datasets used: VOSE for precipitation and temperature (to calculate saturation vapor pressure), PRISM for vapor pressure, LDAS for wind velocity and insolation. Vertical black lines visually divide water years.

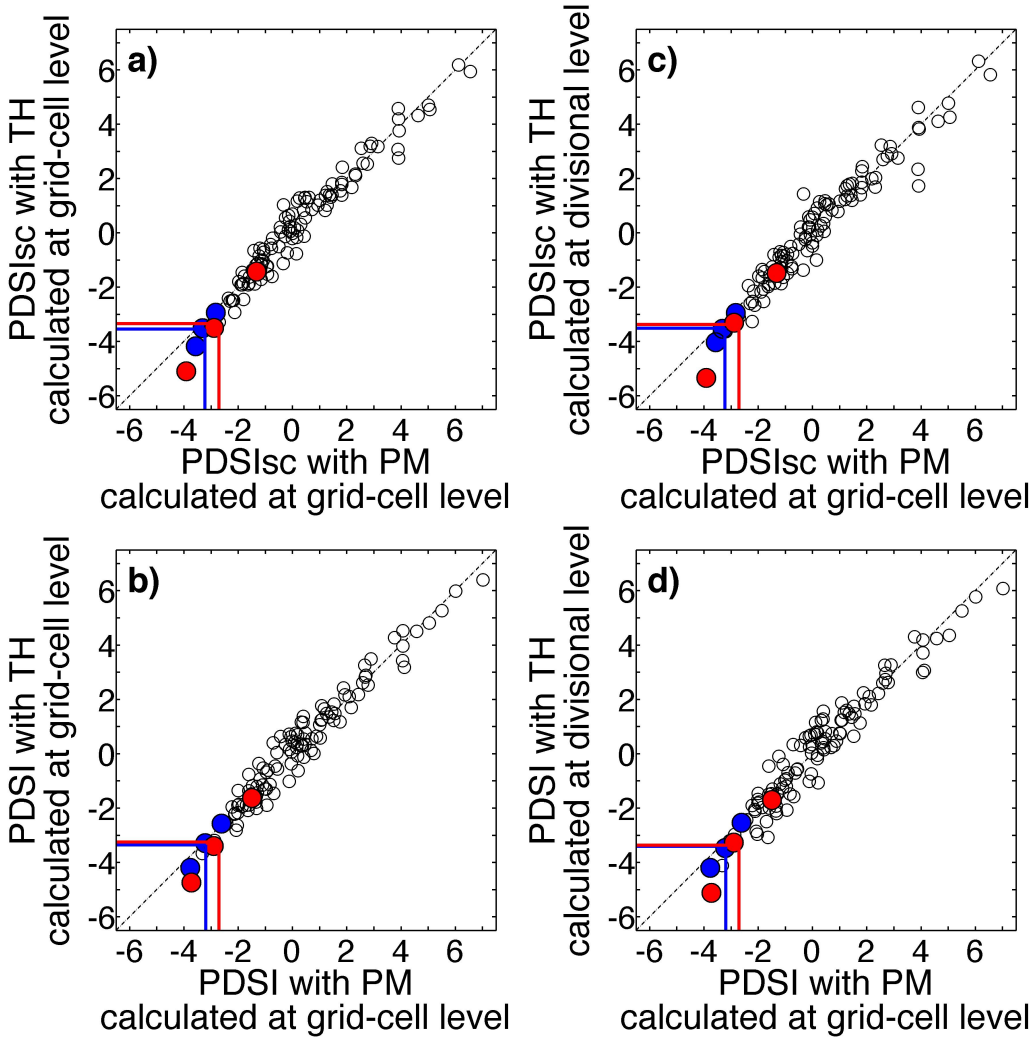

Figure S3. Scatter plots of June–July mean (top panels) $PDSI_{sc}$ and (bottom panels) PDSI for California. PET was calculated with either the (y-axis) Thornthwaite or (x-axis) Penman-Monteith (PM) formulation. $PDSI_{sc}$ and PDSI were calculated at either the (left panels) grid-cell level or (right panels) divisional level (from climate data averaged across each climate division). Red dots: 2012–2014. Blue dots: 2007–2009. The most negative red dot is always 2014 and the most negative blue dot is always 2007. The dashed diagonal line is the 1-to-1 line, and the negative offset of the 2014 dot in the vertical direction within all plots indicates that the 2014 drought is artificially severe when calculated from Thornthwaite PET, especially when climate data are averaged across climate divisions prior to calculation of $PDSI_{sc}$ or PDSI. Red and blue lines: 3-year averages for 2012–2014 and 2007–2009, respectively. All records were standardized to have a mean of zero and a standard deviation of two during 1931–1990. Precipitation and temperature data come from the VOSE dataset to be consistent with the NOAA calculation. For PM PET, vapor pressure comes from PRISM, and wind speed and insolation come from LDAS (or SHEFF for 1901–1947).

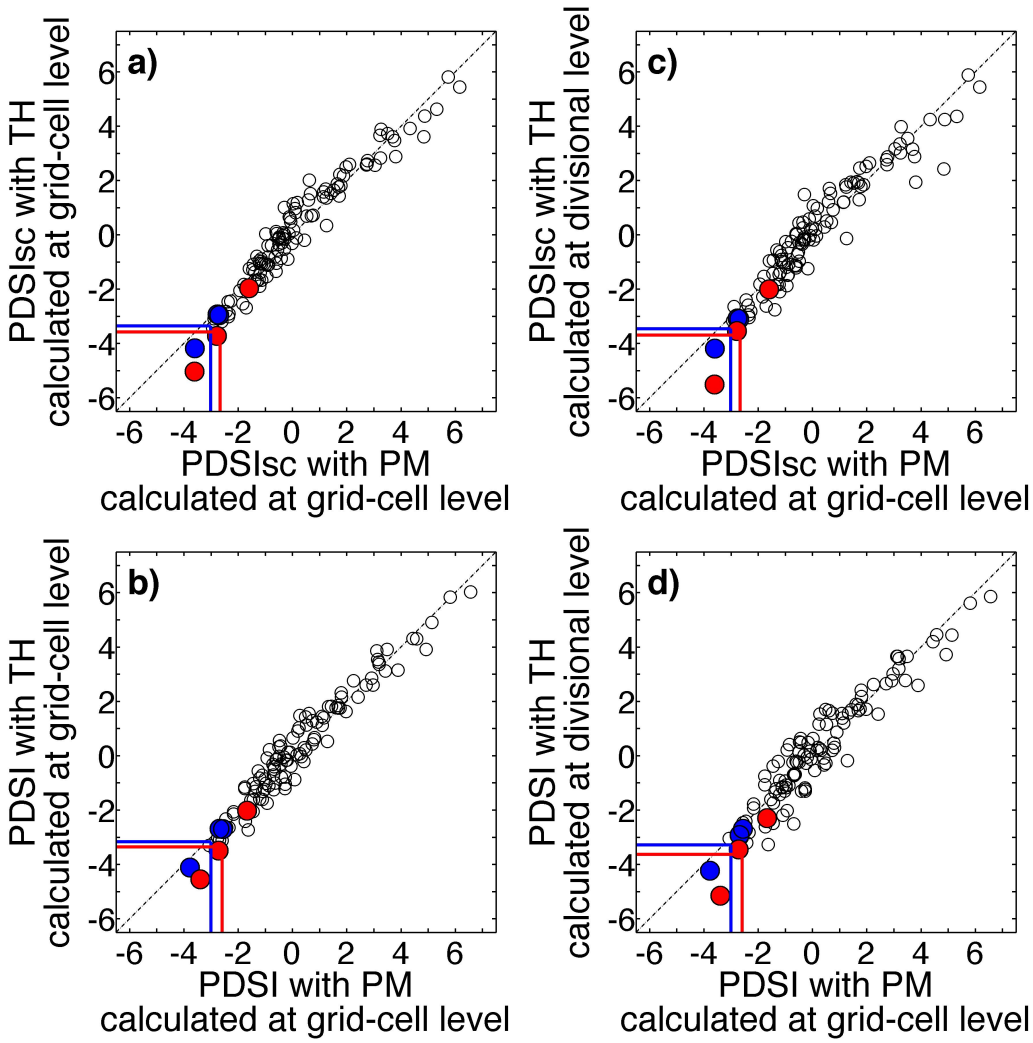

Figure S4. Same as Figure S3, but for only California Climate Divisions 4–7. Scatter plots of June–July mean (top panels) $PDSI_{sc}$ and (bottom panels) PDSI for California. PET was calculated with either the (y-axis) Thornthwaite or (x-axis) Penman-Monteith (PM) formulation. $PDSI_{sc}$ and PDSI were calculated at either the (left panels) grid-cell level or (right panels) divisional level (from climate data averaged across each climate division). Red dots: 2012–2014. Blue dots: 2007–2009. The most negative red dot is always 2014 and the most negative blue dot is always 2007. The dashed diagonal line is the 1-to-1 line, and the negative offset of the 2014 dot in the vertical direction within all plots indicates that the 2014 drought is artificially severe when calculated from Thornthwaite PET, especially when climate data are averaged across climate divisions prior to calculation of $PDSI_{sc}$ or PDSI. Red and blue lines: 3-year averages for 2012–2014 and 2007–2009, respectively. All records were standardized to have a mean of zero and a standard deviation of two during 1931–1990. Precipitation and temperature data come from the VOSE dataset to be consistent with the NOAA calculation. For PM PET, vapor pressure comes from PRISM, and wind speed and insolation come from LDAS (or SHEFF for 1901–1947).

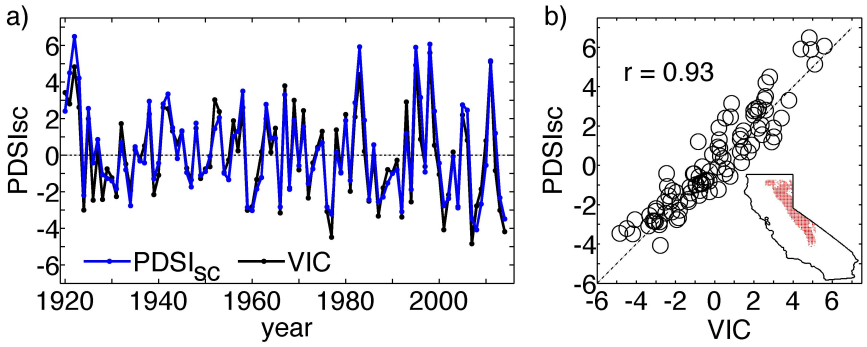

Figure S5. Comparison of (blue) PDSI$_{sc}$ versus (black) modeled VIC soil and snow moisture in the Sierra Nevada Mountains during JJA. The record of VIC soil and snow moisture was transformed to have normal distribution with the same variance as PDSI$_{sc}$ during the 1931–1990 calibration period. The region of focus is identified as the red area on the map inset in (b) and was the study region used by *Mao et al.,* [2015]. In this analysis, PDSI$_{sc}$ was calculated using the same meteorological forcing data used by *Mao et al.,* [2015].

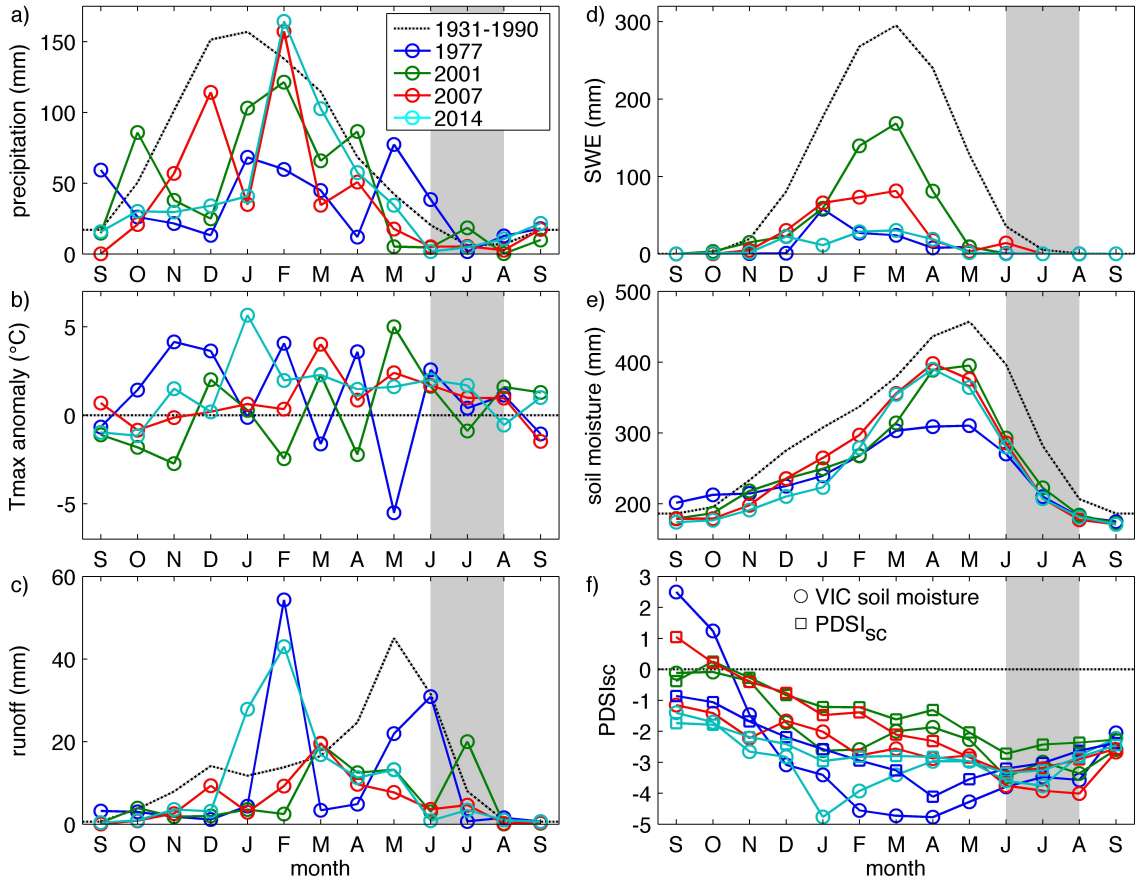

Figure S6. Monthly climate and hydrology characteristics in the Sierra Nevada Mountains during and leading up to the 4 driest years in the VIC soil moisture record. Each colored solid line represents one of the four years and the dotted black line indicates the climatological mean conditions during 1931–1990. In (f), lines with square markers represent the $PDSI_{sc}$ and lines with circular markers represent VIC soil moisture after it has been normalized and calibrated to the distribution of the $PDSI_{sc}$ record. Grey areas indicate the June–August period. All climate data used for this analysis are from *Mao et al.* [2015].

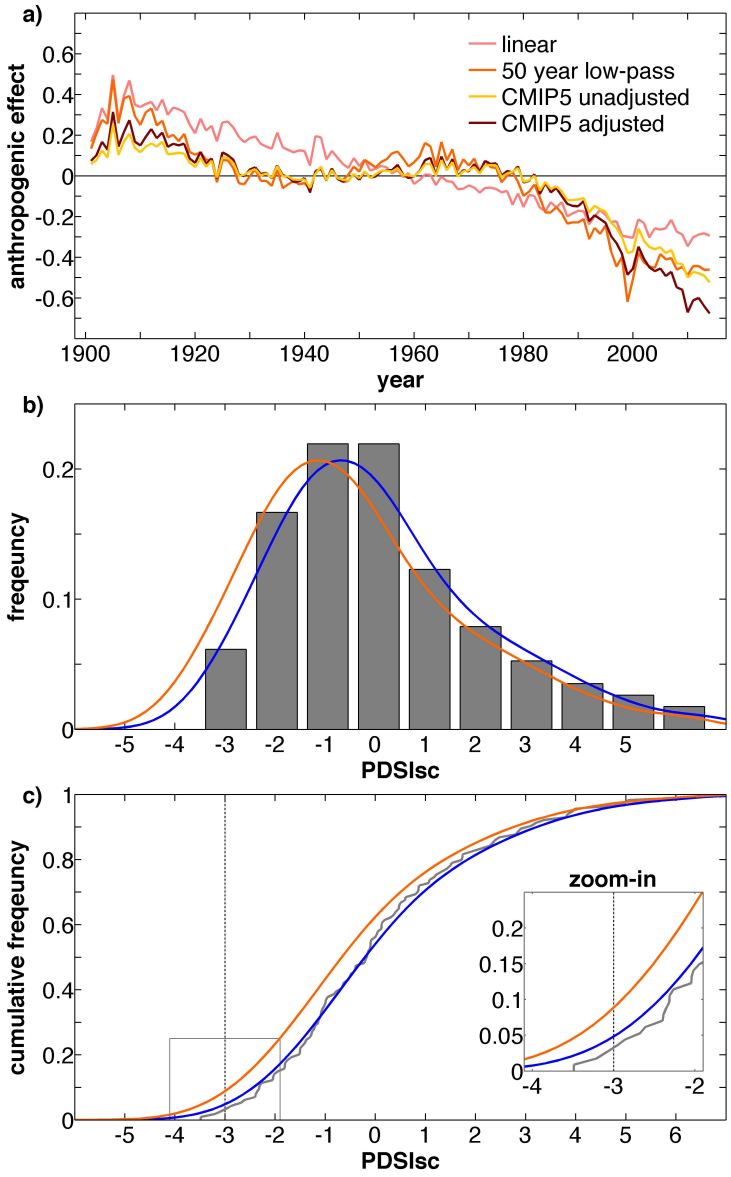

Figure S7. (a) Contribution of each of the four anthropogenic warming scenarios to $PDSI_{sc}$. In 2014, the anthropogenic effect was approximately -0.3 to -0.7. In (b and c), it is assumed that the anthropogenic warming effect in 2014 was the effect illustrated by the 50-year low-pass filter when applied to the VOSE temperature data (-0.46). The grey histogram in (b) and grey empirical cumulative distribution function in (c) represent the distribution of 1901–2014 $PDSI_{sc}$ values when the warming effect is removed. Blue curves are estimates of the distribution function from the kernal density function, meant to represent the hypothetical probability distribution of $PDSI_{sc}$ values in 2014 in the absence of anthropogenic warming. The orange curves are recalculations of this hypothetical $PDSI_{sc}$ distribution shifted uniformly by -0.46, mean to represent the true probability distribution of $PDSI_{sc}$ values in 2014 when anthropogenic warming is included.

References

Allen, R. G., L. S. Pereira, D. Raes, and M. Smith (1998), Crop evapotranspiration-Guidelines for computing crop water requirements-FAO Irrigation and drainage paper 56, 15 pp, Food and Agriculture Organizatoin of the United Nations, Rome. http://www.fao.org/docrep/x0490e/x0490e07.htm#radiation.

Chen, M., P. Xie, J. E. Janowiak, and P. A. Arkin (2002), Global land precipitation: A 50-yr monthly analysis based on gauge observations, *Journal of Hydrometeorology*, *3*(3), 249-266, doi:10.1175/1525-7541(2002)003<0249:GLPAYM>2.0.CO;2.

Compo, G. P., et al. (2011), The twentieth century reanalysis project, *Quarterly Journal of the Royal Meteorological Society*, *137*(654), 1-28, doi:10.1002/qj.776.

Daly, C., W. P. Gibson, M. Dogget, J. Smith, and G. Taylor (2004), Up-to-date monthly climate maps for the coterminous United States, paper presented at Proceedings of the 14th AMS Conference on Applied Climatology, 84th AMS Annual Meeting, American Meteorological Society, Seattle, WA, January 13-16, 2004.

Gupta, S. K., P. W. Stackhouse, S. J. Cox, J. C. Mikovitz, and T. Zhang (2006), Surface Radiation Budget Project completes 22-year data set, *GEWEX News*, *16*(4), 12-13.

Kalnay, E., M. Kanamitsu, R. Kistler, W. Collins, D. Deaven, L. Gandin, M. Iredell, S. Saha, G. White, and J. Woollen (1996), The NCEP/NCAR 40-year reanalysis project, *Bulletin of the American Meteorological Society*, *77*(3), 437-471, doi:10.1175/1520-0477%281996%29077%3C0437%3ATNYRP%3E2.0.CO%3B2.

Kanamitsu, M., W. Ebisuzki, J. Woollen, S.-K. Yang, J. J. Hinilo, M. Fiorino, and G. L. Potter (2002), NCEP-DOE AMIP-II Reanalysis (R-2), *Bulletin of the American Meteorological Society*, *November*, 1631-1643, doi:10.1175/BAMS-83-11-1631.

Lowe, P. R., and J. M. Ficke (1974), The computation of saturation vapor pressure, 27 pp, Monterey, CA.

Mao, Y., B. Nijssen, and D. P. Lettenmaier (2015), Is climate change implicated in the 2013-2014 California drought? A hydrologic perspective, *Geophysical Research Letters*, *42*(8), 2805-2813, doi:10.1002/2015GL063456.

Mesinger, F., G. DiMego, E. Kalnay, K. Mitchell, P. C. Shafran, W. Ebisuzaki, D. Jovic, J. Woollen, E. Rogers, and E. H. Berbery (2006), North American Regional Reanalysis, *Bulletin of the American Meteorological Society*, *87*(3), 343-360, doi:10.1175/BAMS-87-3-343.

Mitchell, K. E., et al. (2004), The multi-institution North American Land Data Assimilation System (NLDAS): Utilizing multiple GCIP products and partners in a continental distributed hydrological modeling system, *Journal of Geophysical Research*, *109*(D7), D07S90, doi:10.1029/2003JD003823.

Monteith, J. L. (1965), Evaporation and environment, *Symoposia of the Society for Experimental Biology*, *19*, 205-224.

Oyler, J. W., A. Ballantyne, K. Jencso, M. Sweet, and S. W. Running (2015), Creating a topoclimatic daily air temperature dataset for the conterminous United States using homogenized station data and remotely sensed land skin temperature, *International Journal of Climatology*, *35*(9), 2258-2279, doi:10.1002/joc.4127.

Penman, H. L. (1948), Natural evaporation from open water, bare soil, and grass, *Proceedings of the Royal Society A: Mathematical, physical and engineering sciences*, *193*, 120-145.

Rodell, M., P. R. Houser, U. Jambor, J. Gottschalck, K. Mitchell, C. J. Meng, K. Arsenault, B. Cosgrove, J. Radakovich, and M. Bosilovich (2004), The global land data assimilation system, *Bulletin of the American Meteorological Society*, *85*(3), 381-394, doi:10.1175/BAMS-85-3-381.

Rohde, R., R. A. Muller, R. Jacobsen, E. Muller, S. Perlmutter, A. Rosenfeld, J. Wutele, D. Groom, and C. Wickham (2013), A new estimate of the average earth surface land temperature spanning 1753 to 2011, *Geoinformatics & Geostatistics: An Overview*, *1*(1), 1-7, doi:10.4172/2327-4581.1000101.

Schneider, U., A. Becker, P. Finger, A. Meyer-Christoffer, M. Ziese, and B. Rudolf (2014), GPCC's new land surface precipitation climatology based on quality-controlled in situ data and its role in quantifying the global water cycle, *Theoretical and Applied Climatology*, *115*(1-2), 15-40, doi:10.1007/s00704-013-0860-x.

Sheffield, J., G. Goteti, and E. F. Wood (2006), Development of a 50-yr high-resolution global dataset of meteorological forcings for land surface modeling, *Journal of Climate*, *19*(13), 3088-3111, doi:10.1175/JCLI3790.1.

Sheffield, J., E. F. Wood, and M. L. Roderick (2012), Little change in global drought over the past 60 years, *Nature*, *491*(7424), 435-438, doi:10.1038/nature11575.

van der Schrier, G., P. Jones, and K. Briffa (2011), The sensitivity of the PDSI to the Thornthwaite and Penman‐Monteith parameterizations for potential evapotranspiration, *Journal of Geophysical Research: Atmospheres*, *116*(D3), D03106, doi:10.1029/2010JD015001.

Vose, R. S., S. Applequist, M. Squires, I. Durre, M. J. Menne, C. N. Williams Jr, C. Fenimore, K. Gleason, and D. Arndt (2014), Improved historical temperature and precipitation time series for US climate divisions, *Journal of Applied Meteorology and Climatology*, *53*(5), 1232-1251, doi:10.1175/JAMC-D-13-0248.1.

Xia, Y., et al. (2012), Continental-scale water and energy flux analysis and validation for the North American Land Data Assimilation System project phase 2 (NLDAS-2): 1. Intercomparison and application of model products, *Journal of Geophysical Research*, *117*(D3), D03109, doi:10.1029/2011JD016051.